RSC Advances

PAPER

View Article Online
View Journal | View Issue

Cite this: *RSC Adv.*, 2023, **13**, 22744

High-performance sorbents from ionic liquid activated walnut shell carbon: an investigation of adsorption and regeneration

Liu Yang, Wang Yungang,* Liu Tao, Zou Li, Bai Yanyuan and Xiu Haoran

In this paper, walnut shells were selected to make activated charcoal using ionic activators. Based on the physical/chemical activation process and the properties of activated carbon products, the Fourier Transform Infrared reflection and Brunauer–Emmett–Teller analysis methods were adopted to comparatively analyse activation principles and pore-structure parameters. Also ciprofloxacin adsorption was compared among various activated carbon. Then, an absence of microporous structure in both walnut shells and their carbonized derivatives was found. Moreover, the specific surface area of activated carbon, prepared *via* KOH wet activation within physical/chemical procedures, attains a noteworthy 1787.06 $m^2\ g^{-1}$, underlining its commendable adsorption performance. The specific surface areas of five distinct activated carbons, processed *via* ionic activation, extend from 1302.01 to 2214.06 $m^2\ g^{-1}$. Concurrently, the micropore volumes span from 0.47 to 0.93 $cm^3\ g^{-1}$. Obviously, the adsorption proficiency of ion-activated carbon markedly exceeds that of carbons activated physically or chemically. Of all materials investigated in this paper, ion-activated carbon D consistently exhibits superior performance, maintaining a ciprofloxacin removal rate nearing 100% at 40 °C. Remarkably, the maximum regeneration frequency of ion-activated carbons can reach up to 10 cycles. In conclusion, these five ion-activated carbons, demonstrating superior pore-structure parameters and adsorptive capacities, outperform those prepared through physical/chemical methods. They emerge as promising contenders for new, high-performing adsorbents.

Received 27th May 2023
Accepted 23rd July 2023

DOI: 10.1039/d3ra03555g

rsc.li/rsc-advances

1 Introduction

Activated carbon, with its unique pore structure and functional groups, possesses commendable thermal stability, chemical stability, high mechanical strength, and reproducibility.[1] As a versatile functional material, it finds widespread applications in various domains such as electrochemistry and environmental protection.[2] Recently, in line with China's rapid development across multiple sectors, the performance requirements and demand for activated carbon have risen, leading to extensive research on the activation and performance of activated carbon.[3]

Zhang and colleagues activated tobacco stem using a physical method, creating activated carbon with several mesopores and micropores *via* the H_2O and CO_2 methods respectively, with mesopores representing a scant 3.85%.[4] On the other hand, Wolfgang and team carried out a physical activation study on diverse agricultural and sideline products, finding the activation effect of the H_2O method to be superior to that of the CO_2 method.[5] Further investigations were conducted by González *et al.* who performed thermal analysis on biomass samples and prepared activated carbon through water vapor gasification. Their results indicated that four types of biomass materials could be employed to create adsorbent materials with differing structural features.[6] In a CO_2 and N_2 atmosphere, Magdziarz *et al.* examined the activation of walnut shell and discovered that the micropores of activated carbon prepared under CO_2 atmosphere were more developed.[7] Román and colleagues activated olive shell by using CO_2, H_2O, or their mixtures, preparing multiple series of activated carbon. They found that CO_2 produced narrow micropores on the olive shell charcoal, a characteristic that amplified over time.[8] Deng *et al.* prepared activated carbon from pineal shell at different KOH/C mass ratios and activation temperatures, reporting that the carbon dioxide adsorption capacity peaked at 7.7 and 5 mmol g^{-1} at 73 K and 298 K, respectively.[9] Alonso *et al.* analyzed the activation of biomass at different proportions of KOH and observed an increase in activated micropores when the agent/material ratio was less than 3. Additionally, they found an increase in the proportion of mesopores in the activated carbon when the ratio was raised.[10] Yu *et al.* evaluated the impact of KOH dosage and other activation factors on the specific surface area and other properties of bamboo chip-activated carbon. They reported that the pore area of the product reached 1490 $m^2\ g^{-1}$, achieved under specific conditions: an agent/material ratio of 0.7,

Key Laboratory of Thermo Fluid Science and Engineering (Ministry of Education), Xi'an Jiaotong University, Xi'an 710049, Shannxi, China. E-mail: ygwang1986@xjtu.edu.c

a temperature of 800 °C, and a duration of 20 min.[11] A similar study by Zhang *et al.* on activated walnut shell using KOH found that at an agent/material ratio of 4, the activated carbon procured at 800–900 °C exhibited optimal performance, boasting a total pore volume of 1.46 mL g^{-1}.[12] Wu and colleagues prepared porous carbon by employing fir wood and pistachio shell as raw materials and activated carbon using water vapor and KOH. They determined that the content of mesopores in activated carbon by water vapor and KOH ranged between 9–15% and 33–49% respectively.[13] Juang *et al.* studied the impact of KOH dosage on the activation of bramble charcoal, revealing that micropores increased when the agent/material ratio was less than 5. However, both micropores and mesopores increased when the ratio exceeded 5.[14] Bardhan *et al.* prepared areca shell-activated carbon *via* chemical activation and found the adsorption capacity of activated carbon to be 381.6, 339.8 and 235.2 mg g^{-1} at 30 °C, 40 °C and 50 °C respectively.[15] Hayashi and team conducted experiments on various types of fruit shells using the K_2CO_3 method and discovered that the activated carbon from all shells performed best at 800 °C.[16] Kim and colleagues examined the adsorption characteristics of trimethoprim onto powdered activated carbon and granular activated carbon, and found that both types of activated carbon reached adsorption equilibrium after 30 and 40 min, respectively.[17] Lastly, Maria *et al.* studied the adsorption capacity of sugarcane bagasse for the removal of ciprofloxacin from water using batch experiments and a fixed bed column. They compared its adsorption performance with a powdered activated commercial carbon and found that both adsorbents achieved a similar percentage removal of about 78%.[18] Pal *et al.* utilized KOH for chemical activation to synthesize activated carbon with a large specific surface area. They also evaluated the thermal conductivity, particle size distribution, pore size distribution, specific surface area, and pore volume of the activated carbon.[19] These studies offer insightful and varied perspectives on the activation of carbon using different raw materials and methods, leading to diverse results in adsorption performance.[20–22]

Given the wealth of research and diverse methods employed in preparing activated carbon, there remains a gap in the use of agricultural and forestry wastes, particularly fruit shells, as raw materials for carbonization. Furthermore, while the main activation methods include physical and chemical processes, they often result in environmental damage, serious equipment corrosion, extensive activator usage, poor economy, and largely produce mesoporous and macroporous activated carbons, with relatively few micropores. Therefore, a pressing need exists for a cost-effective, environment-friendly, and recyclable activation method.[23,24] Ionic liquids, as a new class of green reagents, have seen widespread application in the chemical industry, but their potential in the activation field remains largely unexplored. This paper addresses this gap by employing ionic reagents as activators to activate walnut shells. We compare ionic activated carbon in terms of pore structure parameters, activation mechanisms, and adsorption performance with physically/chemically activated carbon, aiming to identify environment-friendly activation methods and activated carbons with optimal adsorption/regeneration performance.

2 Material and methods

The production process of biomass-activated carbon is typically segmented into two steps: carbonisation and activation. As the surface and internal pores of carbonised biomass charcoal are not properly developed, and the material exhibits almost negligible adsorption capability, the activation of biomass charcoal thus becomes a crucial step in this process.[25]

2.1 Source of raw materials

In this paper, we utilised walnut shells sourced from Weinan, Shaanxi Province, as our primary raw material. Based on response surface analysis, the carbonisation of walnut shell is performed under the following conditions: heating time of 14.8 min, final temperature of 324.7 °C, and holding time of 55.5 min. The particle size of the material used is 2 mm. Subsequent to this, the walnut shell charcoal was activated (Fig. 1).

2.2 Materials and devices

The activated material used in the experiment is the walnut shell charcoal prepared under the optimal carbonisation condition. Carbon particles, of 2 mm size, were ground and screened through a 100-mesh sieve to produce walnut shell charcoal powder. The activated materials of different sizes are then placed in a drying oven and subsequently removed for activation-related experiments to create activated carbon. The primary equipment used in the experiment is detailed in Table 1.

The nitrogen and carbon dioxide utilized in the experiment are standard gases with a purity of 99.99%. For activation purposes, high-purity chemical reagents including KOH, [Bmim]PF_6, [Bmim]BF_4, [Bmim]Cl, and [Hnmp]CH_3SO_3, all with a purity exceeding 99%, are primarily employed.

2.3 Physical/chemical activation conditions

Currently, the primary activation methods include physical and chemical approaches. During chemical activation, chemicals are introduced to the carbon powder, which is then heated

Fig. 1 Walnut shell raw materials.

Table 1 Experimental installation

Instrument	Model	Manufacturer
Air blast drying oven	DHG-9070A	Shanghai Xinyi Instrument Co., Ltd
Constant temperature stirring water bath	HH-1	Shanghai Heheng Instrument Co., Ltd
Electronic analytical balance	ME-55	Mettler Toledo International Limited
pH meter	PHS-2F	Shanghai Yidian Instrument Co., Ltd
Diaphragm vacuum pump	GM-0.5B	Tianjin Jinteng Instrument Co., Ltd
Deionized water machine	AK-RO-C2	Shanghai Yidian Instrument Co., Ltd
BET	BELSORP-Max	McChibeer Co., Japan
Reciprocating thermostatic oscillator	SHZ-C	Shanghai Chuanhong Experimental Instruments Co., LTD
UV/VIS spectrophotometer	UV-3600	Beijing Timesun Measurement and Control Technology Co., Ltd

under an inert atmosphere. Chemical activation methods can be classified broadly into dry and wet activation. On the other hand, physical methods utilize appropriate gases to oxidize the biomass charcoal. The gas reacts with the biomass charcoal at temperatures ranging from 800–1000 °C, consequently leading to the formation of a multitude of complex pore structures.[26–28]

The specific route of chemical activation involves the following steps: (1) dry walnut shell charcoal particles are ground to 100 meshes. (2) A KOH solution with a mass fraction of approximately 85% is prepared. Subsequently, 1 g of charcoal powder is combined with 3 g of KOH powder and KOH reagent. (3) The raw materials for the wet method are sealed with plastic wrap and stirred in a water bath at room temperature. Then the raw materials for the dry/wet method are placed in a drying oven and subjected to a 105 °C heat treatment for 24 h. (4) The dry carbon powder is placed in a tubular furnace under a nitrogen atmosphere and activated at 600 °C for 50 min. (5) The activated carbon is repeatedly washed with deionised water and dried in an air blast drying oven at 105 °C for 12 h to yield C-DKOH and C-WKOH.

The specific route of physical activation involves the following steps: (1) during carbon dioxide activation, 5 g of walnut shell charcoal particles are placed into a tubular furnace. The gas flow is set to 40 mL min^{-1}. Under a nitrogen atmosphere, the temperature is raised to 850 °C at a rate of 20 °C min^{-1}. After maintaining the carbon dioxide temperature for 120 min, it is switched to nitrogen for cooling, producing C-CD. (2) During water vapor activation, the nitrogen flow is set to 150 mL min^{-1}, and the flow of water vapor to 0.2 g min^{-1}. The tubular furnace temperature rises to 850 °C at a rate of 20 °C min^{-1}. After maintaining this temperature for 90 min, the water vapor is turned off, producing C-V. (3) During carbon dioxide/water vapor mixed activation, the carbon dioxide flow is set to 40 mL min^{-1}, and the water vapor flow to 0.41 g min^{-1}. The tubular furnace temperature initially rises to 850 °C at a rate of 20 °C min^{-1} under a nitrogen atmosphere. After switching to mixed gas activation for 60 min, it is again switched to nitrogen. After cooling, C-Mix is obtained (Table 2).

Table 2 Symbol representation of raw materials and activated carbon

Symbol	Abbreviation	Sample
a	WS	Walnut shell
b	WSC	Walnut shell charcoal
c	C-DKOH	KOH dry-method activated carbon
d	C-WKOH	KOH wet-method activated carbon
e	C-CD	CO_2 activated carbon
f	C-V	Vapour activated carbon
g	C-Mix	CO_2&vapour activated carbon

2.4 Ionic activation conditions

Ionic reagents required for ionic activation is a research hotspot in green chemistry. In general, ionic liquid is salt composed of specific organic cations (imidazole, pyrrolidone, pyridine ion, *etc.*) with a large volume of asymmetric structure and inorganic or organic anions (BF_4^-, PF_6^-, $CF_3SO_3^-$, $CF_3CO_2^-$, *etc.*) with small volume. Ionic liquid has unique properties, such as non-flammable, non-volatile, recyclable, low water vapor pressure, difficult to have evaporative boiling, good solubility in most compounds and stable chemical properties. Thus, it is widely used in various fields. Dehydration and carbonisation reactions occur in the catalytic hydrolysis of three elements by ionic liquid.[29] At present, no research has been conducted on ionic activation. This paper aims to analyse the activation effect by using a variety of ion activators.

Ionic reagents employed in this study include [Bmim]BF_4, [Bmim]PF_6, [Bmim]Cl, and [Hnmp]CH_3SO_3, whose structural formulas are illustrated in Fig. 2. Considering the dearth of research on biomass activated by ionic liquid and no report on activation by fruit shell, five feasible experimental schemes were selected after multiple preliminary experiments, based on comprehensive understanding of the aforementioned four ionic liquids. The ionic reagents and their dosages are presented in Table 3.

Ionic activation process: 10 g of 100-mesh walnut shell charcoal powder is weighed and placed into a beaker, followed by dripping the above ionic reagent and a small amount of deionised water into the beaker, which is then sealed with plastic wrap. The beaker is placed into a water bath mixer at 50 °C and stirred for 300 min. A small amount of deionised water is washed and filtered after impregnation. The ionic liquid is extracted from the filtered liquor with ethyl acetate, collected, and reused after centrifugal drying. After being dried in a blast drying oven at 105 °C, the charcoal powder is placed into a tubular furnace. The temperature is increased from room temperature to 600 °C at a rate of 10 °C min^{-1} in a nitrogen

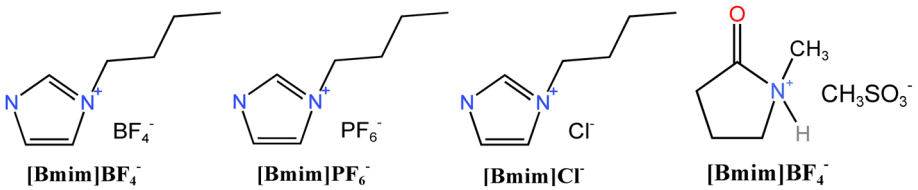

Fig. 2 Molecular structure formula of ion reagent.

Table 3 Ion reagent and its dosage

Sample	Ionic reagents	Dosage
Ion-A	[Hnmp]CH_3SO_3	7.5 g
Ion-B	[Bmim]BF_4	2 g
Ion-C	[Bmim]PF_6	1 g
Ion-D	[Bmim]BF_4 : [Bmim]PF_6 = 3 : 10	1 g
Ion-E	[Bmim]Cl	5 g

atmosphere. The temperature is maintained for 180 min, resulting in the products Ion A–E.

2.5 Ciprofloxacin adsorption experiments

Adsorption experiments on the adsorbents were carried out as follows:

Briefly, 0.01 g of each adsorbent is weighed and placed into a 50 mL conical flask. Then, 20 mL of the CIP (Ciprofloxacin) solution is added to each conical flask at a concentration of 100 mg L^{-1}, and the flask is sealed with plastic wrap and a rubber band. The CIP solution is shaken in a reciprocating thermostatic oscillator at temperatures of 20 °C, 30 °C, 40 °C, 50 °C, and 60 °C and at a speed of 120 rpm. After absorption for 180 min, all the conical flasks are removed, the supernatant is extracted with an injector, and about 10 mL of the solution is filtered into a sample tube *via* a 0.45 μm filter membrane. Variations in concentration are measured using a UV/VIS spectrophotometer.

In these experimental schemes, absorption is measured with a UV/VIS spectrophotometer at a wavelength of 275 nm. Changes in the concentration of the CIP solution are analysed by comparing them to the standard curves. The adsorption capacity of each activated carbon and the corresponding adsorption capacity of the CIP solution are calculated using the following formulas:

$$q_e = \frac{(C_0 - C_e)V}{m} \quad (1)$$

$$P = \frac{C_0 - C_e}{C_0} \times 100\% \quad (2)$$

where q_e represents the adsorption capacity of the adsorbent when the CIP solution was completely absorbed (mg g^{-1}), P represents the removal rate of the CIP solution (%), C_0 represents the initial concentration of the CIP solution (mg L^{-1}), C_e represents the concentration of the CIP solution at the end of adsorption (mg L^{-1}), V represents the volume of the CIP solution (L), and m represents the mass of the adsorbent (g).

2.6 Experiment on the regeneration times of activated carbon

Regeneration of activated carbon involves the removal of adsorbed substances from saturated activated carbon while maintaining the carbon structure, thereby restoring its adsorption capacity and facilitating its reuse. Thermal regeneration of activated carbon is feasible on a large scale, environmentally friendly, exhibits low energy consumption, has a short processing time, and boasts high regeneration efficiency, thereby making it a promising strategy. In the regeneration experiment, the activated carbon with the highest CIP removal rate among Ion A–E was used to investigate the regeneration efficiency and the degradation of regeneration quality with repeated regenerations.

Experimental method: sturated activated carbon was situated in a Buchner funnel lined with filter paper and rinsed several times with deionized water until a neutral pH was reached. Then, it was transferred to a blast drying oven and dried at 105 °C for 24 h. After drying, the activated carbon was weighed, positioned in an alumina boat, and subjected to high-temperature treatment at 350 °C for 2 h in a tube furnace under a nitrogen atmosphere. The regenerated activated carbon was weighed, and adsorption experiments were performed under identical conditions. The adsorption and regeneration experiments were repeated until the activated carbon became completely ineffective.

The formula for calculating the loss rate of regeneration quality of activated carbon is as follows:

$$\eta = \frac{m_1 - m_2}{m_1} \times 100\% \quad (3)$$

where m_1 represents the mass of the saturated activated carbon before regeneration (g), and m_2 represents the mass of the activated carbon after regeneration (g).

The formula for calculating the regeneration rate of walnut shell activated carbon is:

$$\varphi = \frac{C_0 - C_2}{C_0 - C_1} \times 100\% \quad (4)$$

where C_0 represents the initial concentration of the CIP solution (100 mg L^{-1}), C_1 represents the concentration of the CIP solution after the initial adsorption onto activated carbon (mg L^{-1}), and C_2 represents the concentration of the CIP solution after adsorption onto regenerated activated carbon (mg L^{-1}).

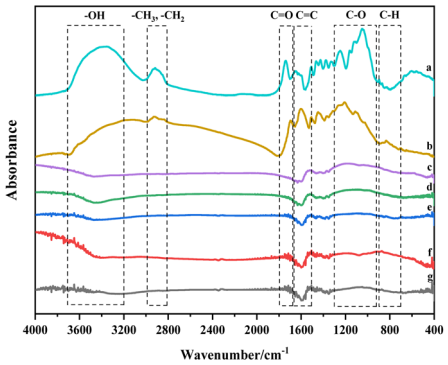

Fig. 3 FTIR spectrotra of physical/chemical activated carbon.

3 Results and discussion

3.1 Analysis of physical/chemical activation

3.1.1 FTIR analysis. FTIR (Fourier Transform Infrared) analysis was conducted to study the chemical structure of the seven samples mentioned above. A total of 32 scans were performed using the potassium bromide powder pellet method. The results, shown in Fig. 3, indicate that WS and WSC possess noticeable functional groups, including hydroxyl, aliphatic groups, oxygen-containing functional groups, and aromatic hydrocarbons. Activated carbon displays fewer functional groups with a relatively flat curve. The following discussion examines cellulose, hemicellulose, and lignin in the walnut shell.

Walnut shell's cellulose, hemicellulose, and lignin are composed of various functional groups found in olefins, esters, aromatics, ketones, and alcohols. Yang *et al.* investigated the three components using FTIR, revealing distinct infrared structures for each. Cellulose demonstrates the highest infrared absorbance for –OH and C–O, while hemicellulose comprises –OH, C–O, and C=O compounds.[30] Compared to cellulose and hemicellulose, lignin shows significant differences in the infrared spectrum within the characteristic range (730–1830 cm^{-1}). Lignin is a compound rich in $–O–CH_3$, C–O–C, C=C, and C–H. Carbonisation involves breaking C–O–C and C–H and transforming aromatic rings. As lignin is rich in the mentioned functional groups within its characteristic area, its transformation and reactions primarily influence the formation of the graphite structure during carbonisation and activation.[31]

The histogram in Fig. 4 displays the normalized changes in functional groups within each characteristic area across the seven samples. The normalization process for all data is as follows: The integral area of the spectral peak associated with

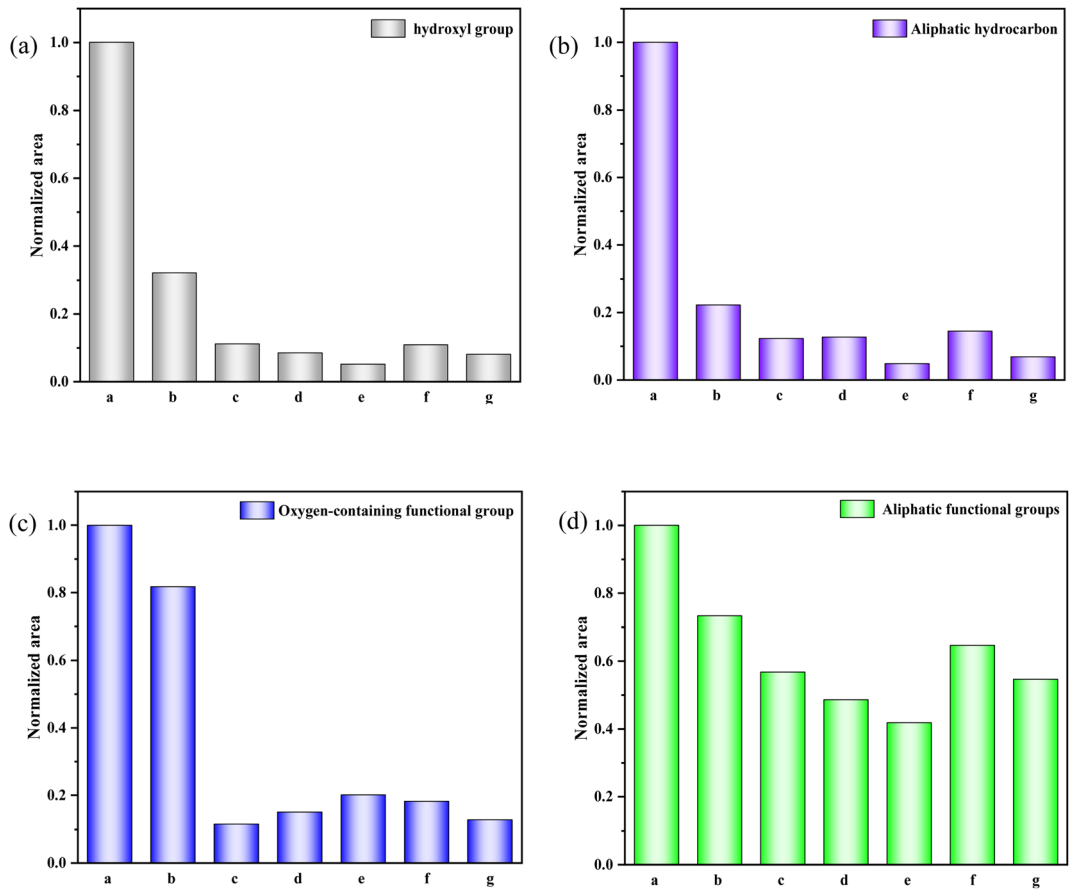

Fig. 4 Evolution of various functional groups during physical/chemical activation of walnut shells. (a) 400–1300 cm^{-1}. (b) 1300–2000 cm^{-1}. (c) 2000–3000 cm^{-1}. (d) 3000–4000 cm^{-1}.

the functional group of the walnut shell is set as 1, and normalization is carried out on the integral area of the spectral peaks of functional groups of other samples.

Fig. 4(a) provides a quantitative analysis of each sample's hydroxyl group. Examining the change in hydroxyl content during carbonisation and activation reveals that with increasing temperature, significant evaporation of water in the walnut shell sample occurs during carbonisation, and the bound hydroxyl decomposes. This leads to a marked reduction in hydroxyl content and the formation of pore structure. Hydroxyl content slightly decreases during activation, which is due to the decomposition of the majority of bound hydroxyl groups.

Aliphatic functional groups, primarily composed of $-CH_3$ and $-CH_2$, fall within the 2800–3000 cm^{-1} range. The histograms in Fig. 4(b) illustrate changes in these aliphatic functional groups. During carbonization, $-CH_3$ and $-CH_2$ as highly active functional groups exhibit strong reactivity, resulting in significant consumption. During activation, the content of these aliphatic functional groups diminishes slightly as aliphatic hydrocarbons are essentially depleted.

The variation in oxygen-containing functional groups during carbonization is marginal, as depicted in Fig. 4(c). These functional groups exhibit low activity during carbonization at lower temperatures, and other functional groups transform into oxygen-containing functional groups in this stage. During activation, the differences in the content of oxygen-containing functional groups among activated carbon samples are not significant. However, this content profoundly affects the chemical adsorption and other properties of activated carbon.[32]

Fig. 4(d) presents the decline in aromatic functional groups during both carbonization and activation. A minor difference in the content of aromatic compounds can be observed among activated carbon samples. The content of aromatic compounds in the C-Mix sample is the lowest, suggesting that the greatest burst size of aromatic functional groups occurs during the activation of mixed gas. Consequently, the formed activated carbon exhibits a stable structure and a high degree of graphitization.

3.1.2 BET analysis. The ASAP020 physical adsorption tester from Mike Instruments was used to analyze the activated carbon samples in this paper. The BET (Brunauer–Emmett–Teller) method was employed to calculate the specific surface area of the activated carbon, the t-plot method was used to determine the micropore volume and specific surface area, and the BJH (Barrett–Joyner–Halenda) method was used to calculate the pore size distribution and average pore size. The nitrogen adsorption–desorption curves are presented in Fig. 5, and the pore structure parameters of the activated carbon samples are listed in Table 4.

The curves for walnut shell and walnut shell charcoal, shown in Fig. 5, are indicative of typical non-porous material curves, demonstrating minimal adsorption and desorption. Activated carbon samples c and d, activated *via* dry and wet chemical methods, were further analyzed. When P/P_0 is less than 1, the nitrogen adsorption capacity increases rapidly, suggesting a microporous structure in the chemically activated carbon. When P/P_0 exceeds 0.1, capillary condensation is observed in both curves, suggesting that the adsorption and desorption curves do not overlap and a hysteresis loop is evident.

The C-WKOH and C-DKOH samples showed that the specific surface area, pore volume, and micropore volume of C-WKOH are higher than those of C-DKOH. The average pore size of activated carbon by the chemical method is 1.79 and 2.03 nm. Thus, C-WKOH has a rich microporous structure with fewer, smaller mesopores and robust adsorption. Conversely, while C-DKOH also shows strong adsorption, its average pore size slightly exceeds 2 nm, indicating significant mesopore production during activation, and the activation degree of C-DKOH is much lower than that of C-WKOH.

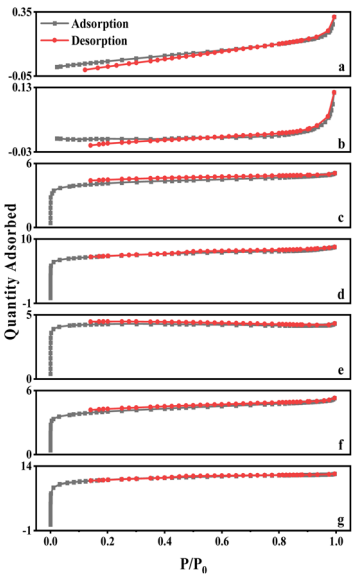

Fig. 5 Adsorption–desorption isotherm of physical/chemical activated carbon.

Table 4 Structural parameters of the physical/chemical activated carbon pores

Activated carbon	Specific surface area/m^2 g^{-1}	Pore volume/cm^3 g^{-1}	Micropore volume/cm^3 g^{-1}	Average pore size/nm
C-DKOH	885.23	0.46	0.32	2.03
C-WKOH	1787.06	0.76	0.56	1.79
C-CD	807.90	0.43	0.38	1.86
C-V	512.08	0.27	0.14	2.30
C-Mix	1214.06	0.63	0.51	2.11

When comparing C-CD, C-V, and C-Mix, it can be seen that C-CD has a specific surface area of 807.9 m^2 g^{-1}, with more micropores, and the average pore size is only 1.86 nm. The CO_2 activation process produces a significant quantity of micropores. C-V has the smallest specific surface area of 512.08 m^2 g^{-1}, and its average pore size is 2.3 nm. During the H_2O activation process, pore formation and expansion lead to a larger pore size and poorer adsorption capacity. The specific surface area of C-Mix is 1214.06 m^2 g^{-1}, and its adsorption capacity is good. This suggests that the mixed gas activation process, involving pore formation by CO_2 and pore expansion by H_2O, results in some micropores being oxidized and expanded to mesopores.

3.1.3 Comparison of physical/chemical activation. In comparing physical and chemical activation methods, it appears that dry and wet chemical activation methods can produce activated carbon with a high specific surface area at a lower activation temperature and provide better cost performance. In contrast, the physical activation method is inferior to the chemical method in producing activated carbon. CO_2 activation produces more micropores but is more expensive, making it suitable mainly for laboratory research. H_2O activation, which is widely used in the industry due to its cost-effectiveness, typically produces poorer activation results and more mesopores in the activated carbon. However, when the specific surface area and adsorption requirements for activated carbon are low, H_2O activation can be chosen. Of the methods evaluated, wet method activation of walnut shell proves to be the optimal choice due to its superior specific surface area, micropore volume, and average pore size, rendering it suitable as an adsorbent. The mixed gas activation method takes second place, with its physical adsorption capacity only second to wet activation and a considerable micropore volume.

3.2 Analysis of ionic activation

3.2.1 FTIR analysis. The paper has discussed in detail the decomposition and transformation of functional groups associated with three elements during the processes of carbonisation and activation. Ionic activation is broadly similar to physical and chemical activation. Carbonisation primarily involves the breakdown of C–O–C and C–H bonds and the transformation of aromatic rings, with the main difference being the hydrolysis change of cellulose. Under the influence of ionic liquid, cellulose functional groups undergo a hydrolysis reaction, producing glucose. This hydrolysis reaction ceases during high-temperature activation (Fig. 6).

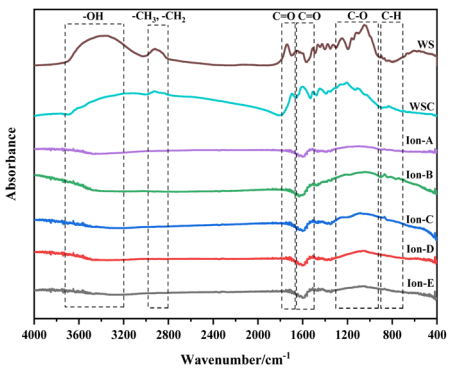

Fig. 6 FTIR spectrum of ionic activated carbon.

The curve fitting and analysis of Ion A–E materials were conducted using PeakFit, and the results normalised for the areas of multiple fitting peaks in the characteristic region. The analysis and comparisons are shown in Fig. 7.

Fig. 7(a) shows a quantitative analysis of the hydroxyl group of each sample using the FTIR spectrum. The analysis of the hydroxyl group content change during carbonisation and activation indicates a rapid decrease in the walnut shell sample with increasing temperature. A small difference in the content of the hydroxyl group is observed in the activated carbon samples Ion A–E. Hydroxyl has high reactivity, with its consumption and production processes occurring simultaneously. The primary decomposition process of hydroxyl is carbonisation. Its decline during the activation stage slows, but it is still evident. The ionic activated carbon shows a lower hydroxyl content than that of physical–chemical activated carbon, suggesting a high degree of hydroxyl decomposition. The pore structure forms as hydroxyl produces water vapor, creating a high specific surface area.

Fig. 7(b) presents a histogram of the change in aliphatic functional groups. The trend is similar to that of the hydroxyl group. The consumption of aliphatic hydrocarbons is high during the carbonisation stage, and the content of its functional group drops significantly. During activation, the change in the aliphatic functional group content is minimal, and aliphatic hydrocarbons are completely decomposed at 300–400 °C.

Fig. 7(c) shows a histogram of the change in the total quantity of oxygen-containing functional groups. As the reaction progresses, the content of oxygen-containing functional groups displays a decreasing trend. The decomposition and production reactions of oxygen-containing functional groups occur simultaneously during carbonisation and activation. The normalised area of oxygen-containing functional groups is only 0.18 during the carbonisation stage. The reaction activity at low temperatures is low, causing slow decomposition of the functional groups and production of oxygen-containing functional groups. As the activation reaction temperature increases, the reaction activity also increases, leading to a significant decrease in oxygen-containing functional groups.

Fig. 7(d) demonstrates the change in the normalised area of aromatic functional groups with the ionic activation of walnut shell. The aromatic functional groups show a decreasing trend during activation and carbonisation. However, their changes vary greatly under different activation techniques. The content of aromatic compounds is high, being the primary component of lignin and the structural backbone of the walnut shell material. The reaction of aromatic compounds will form the structural body of carbon and activated carbon. Ionic activation of walnut shell leads to the creation of activated carbon with a stable structure and a high degree of graphitisation. When compared with physical and chemical activation, ionic activated carbon exhibits a significant difference in the normalised area

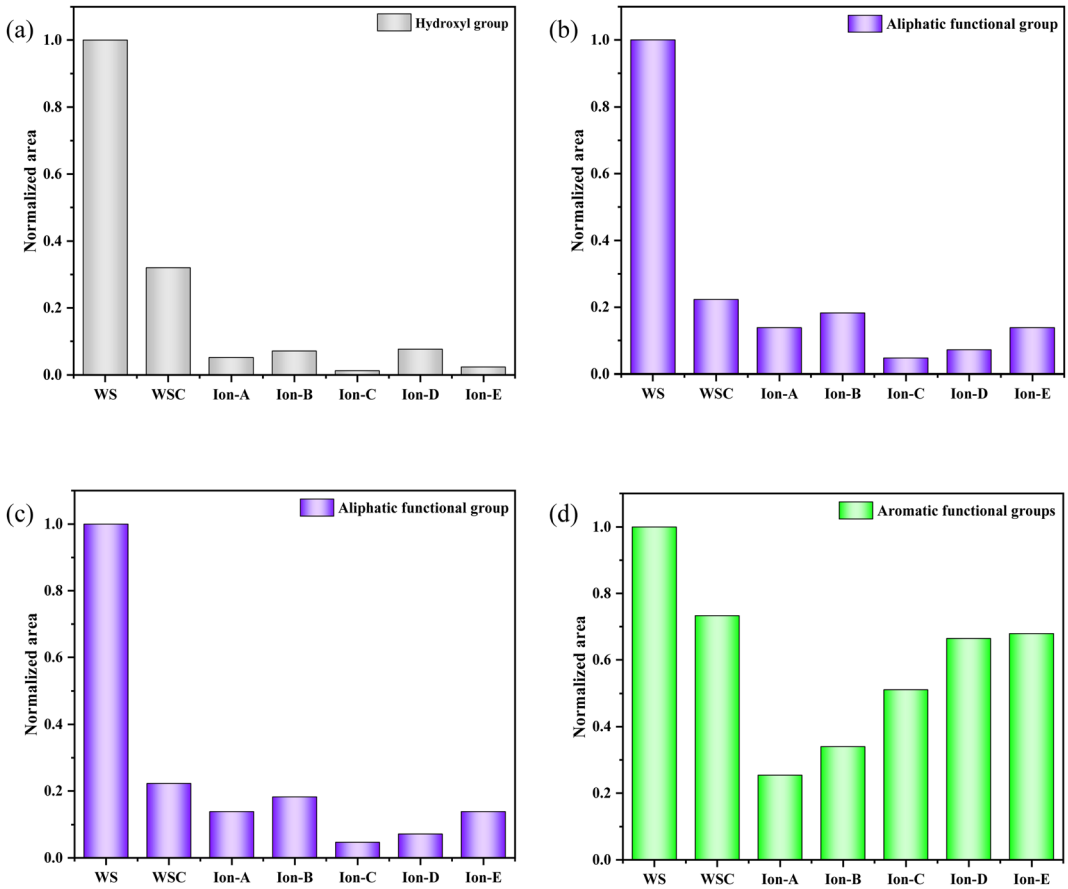

Fig. 7 Evolution of various functional groups during ion activation in walnut shells. (a) 400–1300 cm^{-1}. (b) 1300–2000 cm^{-1}. (c) 2000–3000 cm^{-1}. (d) 3000–4000 cm^{-1}.

of aromatic hydrocarbons but is slightly superior to activated carbon created by physical and chemical activation.

3.2.2 BET analysis. Fig. 8 illustrates the adsorption isotherm of ionic activated carbon, while Table 5 details the pore structure of ionic activated carbon.

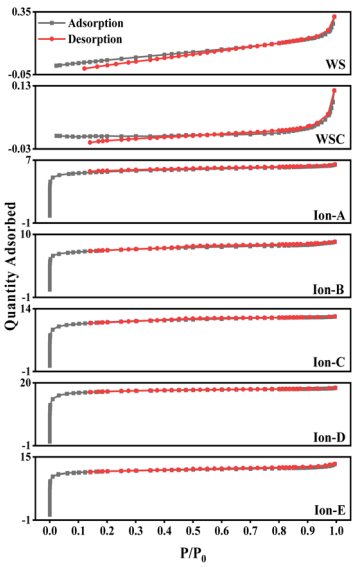

Fig. 8 Adsorption–desorption isotherm of ion-activated carbon.

As seen in Table 5, ionic activation results in a rich microporous structure, with an average pore size between 1.81 and 2.14 nm. This suggests that mesopores resulting from ionic activation are fewer and relatively smaller. The small average pore size indicates a robust adsorption capacity. The specific surface area of ionic activated carbon ranges from 1302.01 to 2214.06 $m^2\ g^{-1}$, and the micropore volume spans from 0.47 to 0.93 $cm^3\ g^{-1}$. Generally, these structural parameters of ionic activated carbon outperform those of carbon activated by traditional methods. Common market-available biomass-activated carbon has a specific surface area between 500 and 1700 $m^2\ g^{-1}$.

Among all, Ion-D, prepared using a mixture of $[Bmim]PF_6$/$[Bmim]BF_4$ ionic liquids, demonstrates excellent structural parameters. It boasts a specific surface area of 2214.06 $m^2\ g^{-1}$, a micropore volume of 0.93 $cm^3\ g^{-1}$, and an average pore size of 1.81 nm. Considering its exceptional adsorption effect, low production cost, and superior adsorption performance, Ion-D can be effectively used as activated carbon for treating waste smoke and wastewater.

Fig. 8 also displays the isotherms for Ion A–E. When the relative pressure P/P_0 is less than 1, the nitrogen adsorption capacity rapidly increases, signifying a microporous structure in Ion A–E. When P/P_0 is more than 0.1, adsorption curves align with desorption curves, with capillary condensation observed,

Table 5 Structure of the pore parameters of ion-activated carbon

Ionic activated carbon	Specific surface area/m^2 g^{-1}	Pore volume/cm^3 g^{-1}	Micropore volume/cm^3 g^{-1}	Average pore size/nm
Ion-A	1302.01	0.67	0.47	2.14
Ion-B	1817.92	0.77	0.62	1.82
Ion-C	1974.04	1.05	0.83	2.04
Ion-D	2214.06	1.16	0.93	1.81
Ion-E	2007.90	1.04	0.88	1.93

similar to earlier physical/chemical methods. Interestingly, no hysteresis loop is present. The analysis reveals that the physical adsorption properties of ionic activated carbon follow the order from largest to smallest: Ion-D > Ion-E > Ion-C > Ion-B > Ion-A.

The adsorption capability of Ion-D exceeds that of other ionic carbons. Furthermore, the adsorption isotherm for Ion B–E surpasses that of the optimal method used in physical/chemical activation. While Ion-A's activation effect is somewhat inferior, it is still considerably better than those achieved through general physical/chemical activation methods.

3.3 SEM analysis of activated carbon

Fig. 9 showcases the surface morphology of samples produced by both conventional activation and ionic activation methods. Specifically, Fig. 9(a) and (b) correspond to carbon activated by the KOH wet method (referred to as C-WKOH), while Fig. 9(c) and (d) represent Ion-D.

As observed in Fig. 9, the surface of C-WKOH exhibits a honeycomb-like structure due to etching, with a relatively rough surface hosting a large number of mesopores. Upon closer examination, a channel structure is visible on the

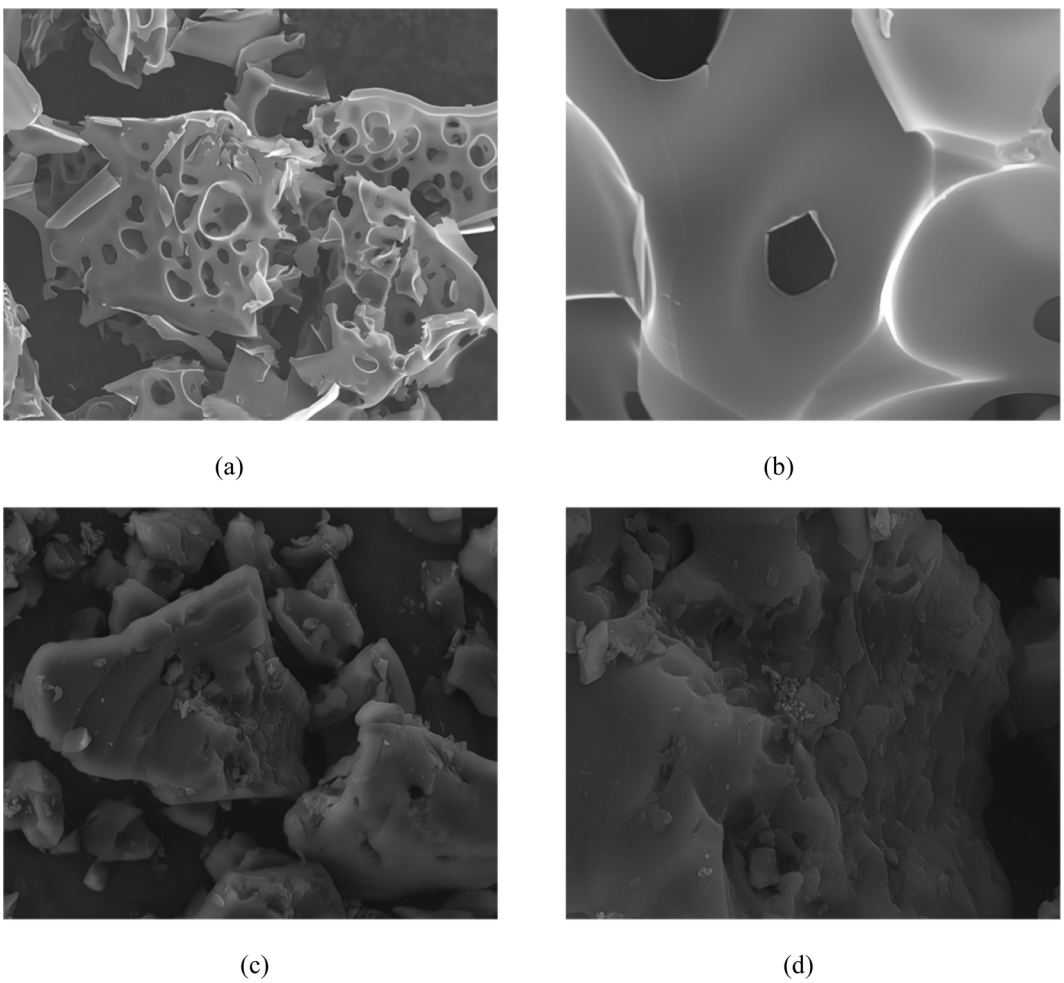

Fig. 9 The surface morphology of wet activated carbon and ionic activated carbon D. (a) C-WKOH at 1 K magnification. (b) C-WKOH at 10 K magnification. (c) Ion-D at 1 K magnification. (d) Ion-D at 10 K magnification.

activated carbon's surface. These channels connect to the internal microporous structure, which is found to be abundant based on pore parameter analysis, consequently contributing to a large specific surface area.

Contrarily, the surface of Ion-D appears relatively dense with fewer visible pores. Upon analysis, a considerable quantity of micropores and a minimal number of mesopores are discovered. Furthermore, a complex microporous structure is detected inside the activated carbon. Complementary BET results suggest that these mesopores, upon extending into the activated carbon, reduce in size and contribute to forming a complex micropore network structure, thereby increasing the specific surface area.

In comparison to activated carbon prepared *via* physical/chemical methods, ionic activated carbon showcases a denser surface with fewer mesopores yet larger micropore volume and quantity. Additional microporous structures are also found internally. This results in a larger specific surface area and superior adsorption performance, particularly towards small-molecular gas/liquid substances.

3.4 Ionic activation mechanism analysis

Fig. 10 outlines the main principles of ionic activation, which play a crucial role in the treatment of cellulose, especially in the context of walnut shell-based biomass char. This process comprises three key steps:

Firstly, at room temperature, ionic reagents are capable of hydrolyzing the residual cellulose in walnut shell-based biomass char. This hydrolysis is rather comprehensive, as inferred from infrared analysis, resulting in the creation of pores and a minor quantity of glucose. Therefore, when dealing with walnut shell-based biomass, the ideal final temperature during carbonization should be approximately 324.7 °C, close to the threshold for complete cellulose decomposition. This approach permits the partial decomposition of remaining cellulose by ionic reagents, contributing to micropore formation. Selecting this temperature prevents an excessive amount of cellulose in the biomass char if the carbonization temperature is too low, which could lead to an overabundance of mesopores and macropores and even pore collapse.

Furthermore, as depicted in Fig. 7's hydroxyl decomposition analysis, ionic reagents aid in the decomposition of hydroxyl groups in walnut shell-based biomass, surpassing the degree of decomposition attainable by physical/chemical activation methods. Water vapor generated during this decomposition process assists in pore formation, leading to an increased pore count in ionic activated carbon.

Lastly, ionic reagents facilitate the decomposition and transformation of aromatic functional groups. This results in a significant portion of lignin being converted into a carbon structure. The conversion degree is high, leading to the formation of ionic activated carbon exhibiting a high graphitization degree and structural stability, and the pore structure is less likely to incur damage.

Cellulose, a vital component of walnut shells, decomposes into gas at high temperatures during physical/chemical activation. After the walnut shell undergoes low-temperature carbonization, some cellulose persists. At this juncture, the residual cellulose can be hydrolyzed by ionic reagents at 50 °C for 300 min, leading to the formation of activated carbon pores. Following this, at 600 °C for 180 min, unstable substances in the walnut shell carbon undergo decomposition or transformation into physically/chemically stable substances, yielding activated carbon that is both stable and rich in micropores.

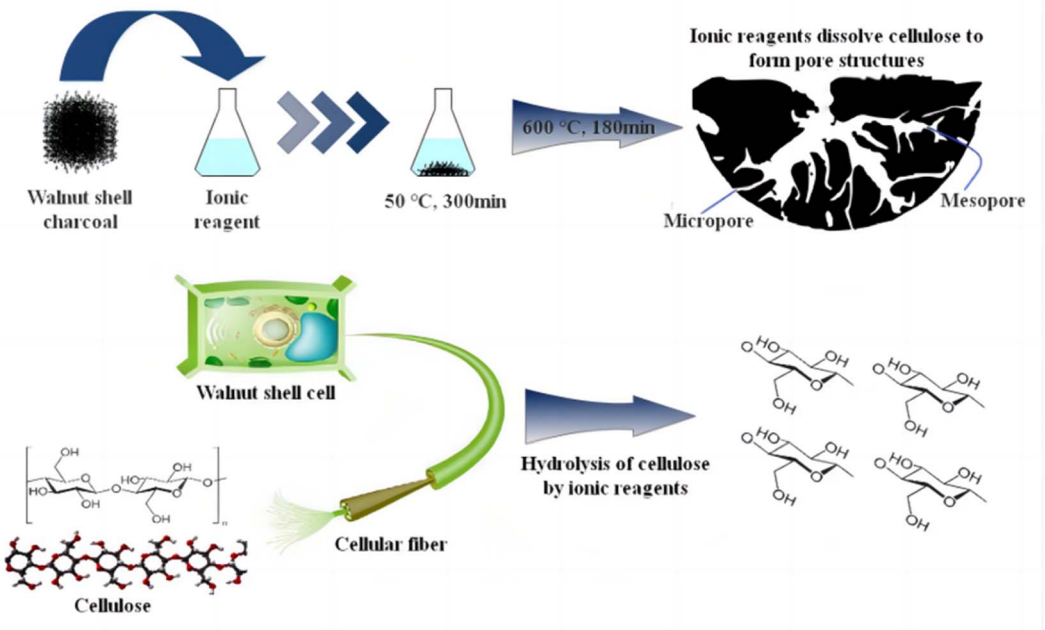

Fig. 10 Mechanism of ion activation process.

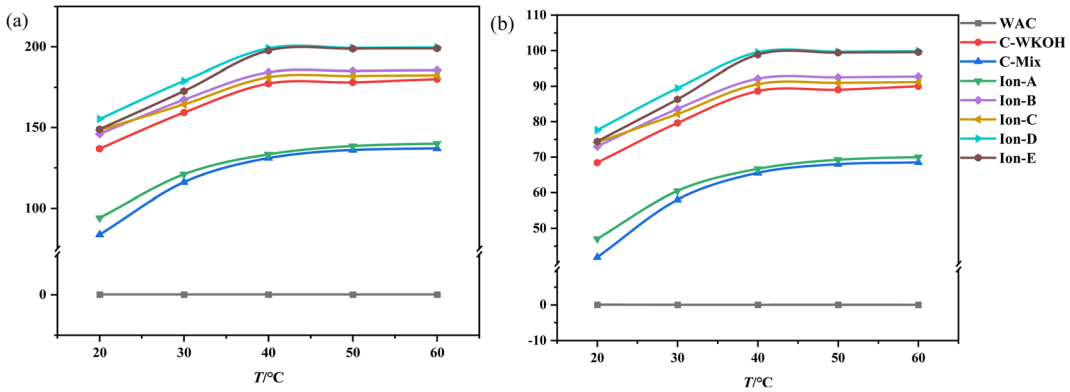

Fig. 11 Effects of temperature on the adsorption of activated carbon. (a) Effects of temperature on the adsorption capacity. (b) Effects of temperature on the removal rate.

3.5 CIP adsorption experimental results and analysis

Fig. 11(a) illustrates changes in adsorption capacity as a function of temperature, while Fig. 11(b) shows the rate of CIP solution removal at various temperatures. These figures indicate that temperature plays a significant role in the adsorption capacity of the activated carbons studied.

When temperature was held constant, the adsorption capacity of WSC remained near zero. Below 40 °C, significant differences in adsorption capacity were observed between all types of activated carbon. As the temperature increased, the adsorption capacity of all except WSC increased noticeably. WSC's adsorption capacity showed minimal growth after 40 °C.

Meanwhile, the adsorption capacities of ionic activated carbons (Ion A–E) continued to rise with temperature and maintained a high level. Ion-D, in particular, consistently demonstrated the highest adsorption capacity within the studied temperature range. Between 20 °C and 40 °C, the removal rate of the CIP solution with Ion A–E was above 73%, and it was as high as 77.65% with Ion-D. The performance of the activated carbons sorted by their adsorption capacity follows this pattern: Ion-D > Ion-E > Ion-B > Ion-C > C-WKOH > Ion-A > C-Mix. This suggests that the adsorption process by activated carbons is highly influenced by temperature within the investigated range. An increase in temperature can enhance adsorption by accelerating the motion of small CIP molecules in fluid, leading to more frequent contact with WSC and subsequently increasing adsorption capacity.

In the temperature range of 40–60 °C, the adsorption capacity of activated carbon began to stabilize, and the removal rate of the CIP solution with Ion-B–E was above 90%. Remarkably, the removal rate with Ion-D or Ion-E reached up to 99.5% or 98.83%, almost completely removing the CIP solution. The removal rate with C-WKOH was 88.62%, and the performance of C-Mix or Ion-A was relatively poor. The removal rate did not increase significantly with temperature, indicating effective adsorption at 40 °C and suggesting that high temperatures causing heat loss can be avoided.

Regarding the pore structure, it is formed by etching both the surface and interior, and controlling the activation process can be challenging. The activation process can easily generate mesopores, which can impact the volume and adsorption performance of micropores. Due to the distinct activation principles, ionic activated carbon features more micropores and fewer mesopores. Thus, it can potentially be used as a new high-performance adsorbent.

3.6 Experimental results analysis of regeneration

3.6.1 Results of ion-activated carbon regeneration experiment. Fig. 12 visualizes the effect of using ion-activated carbon D as the regeneration material on the activated carbon's regeneration efficiency and mass loss rate. In the initial ten regeneration cycles, the regeneration efficiency consistently remains above 88%, while the mass loss rate varies slightly between 22.37% and 26.69%. This suggests that the porous structure of the activated carbon is largely preserved, allowing for repetitive regeneration while maintaining a desirable CIP removal rate. However, during the 11th regeneration cycle, a steep decline in both regeneration efficiency and mass loss rate is observed. Regeneration efficiency drops to 74.55%, indicating significant degradation as the microporous structure begins to collapse, and the specific surface area decreases rapidly.

Fig. 13 shows morphological images of ion-activated carbon D before and after eleven regeneration cycles. There's a notable

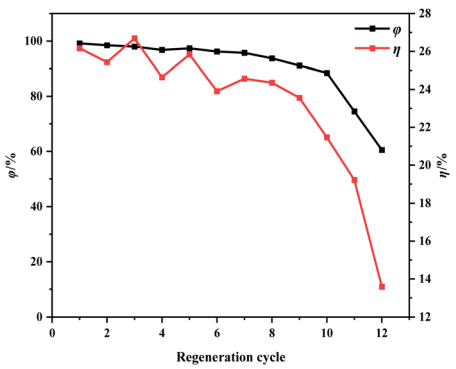

Fig. 12 Effect of regeneration cycles on regeneration efficiency and mass loss rate of ion-activated carbon.

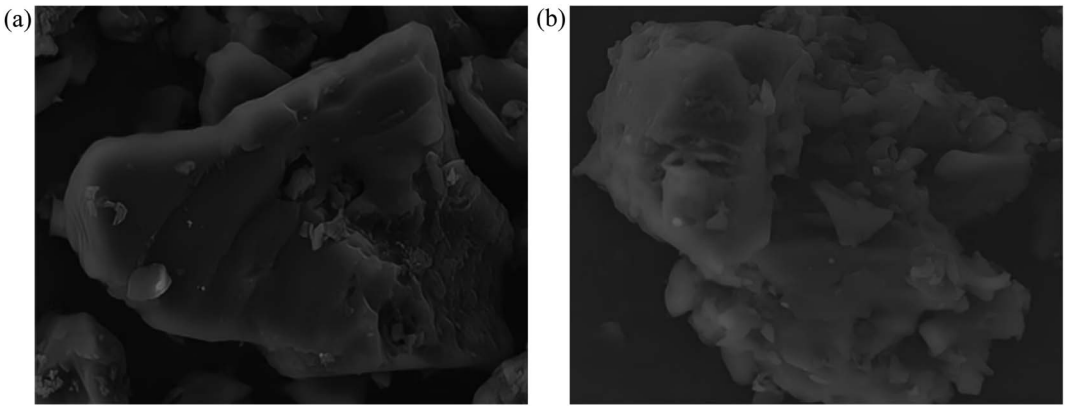

Fig. 13 Microstructure comparison of activated carbon after 11 regeneration cycles. (a) Before regeneration. (b) After 11 regeneration cycles.

transformation in the surface morphology of the activated carbon. Before regeneration, the activated carbon displays a rather dense surface with visible micro-pores, pointing to a primarily intact structure. However, after eleven successive regeneration cycles, the activated carbon undergoes particle aggregation and pulverization. The surface of the activated carbon displays an increased number of larger pores and particles, resulting in a significant reduction in specific surface area, indicative of a severe loss of activity and substantial degradation of the activated carbon.

3.6.2 Analysis of ion-activated carbon regeneration mechanism. Generally, biomass-based activated carbons have a limited number of regeneration cycles, typically between 3 and 5 cycles. The activated carbons with stable structures and superior performance can withstand thermal regeneration for about 6 to 7 cycles, with an initial regeneration efficiency typically ranging from 90% to 95%, and a final regeneration efficiency of approximately 80% before degradation.[33,34] The limited number of regeneration cycles and reduced regeneration efficiency in commonly available activated carbons can be attributed to their low yield, inadequate graphitization, low porosity, and unstable pore structure, which make them prone to pore collapse.

During the regeneration process of shell-based ion-activated carbon post-CIP adsorption, the residual CIP within the interstitial spaces decomposes, generating water vapor and volatile gases. These react with carbon molecules, causing surface corrosion and damage to the pore structure of the ion-activated carbon, significantly impacting its lifespan. As shown in Fig. 13, the shell-based ion-activated carbon exhibits an impressive regeneration cycle capacity of up to 10 cycles, with an initial regeneration efficiency of 98.64% and a final regeneration efficiency of 88.04%. However, during the 11th regeneration cycle, the pore structure of the ion-activated carbon collapses, while still achieving a regeneration efficiency of 74.55%.

The outstanding regenerative performance of shell-based ion-activated carbon can be attributed to its underlying mechanism. The key contributing factors to this mechanism are the use of ion reagents, which enhance the decomposition of aromatic functional groups, leading to almost complete conversion of lignin into the fixed carbon component of the activated carbon. This positive aspect results in a higher yield of activated carbon and reduces the effect of mass loss during the regeneration process. Additionally, as depicted in Fig. 7, shell-based ion-activated carbon exhibits a higher degree of graphitization and a more stable structure. This increased stability of the pore structure during the heat-driven regeneration process decreases the propensity to collapse. Consequently, even after the regeneration treatment, the regeneration efficiency of the activated carbon continues to be maintained at a high level.

4 Conclusion

This paper delves into the impact of physical/chemical/ionic activation on walnut shells and contrasts their activation mechanisms, pore structure parameters and regeneration mechanisms. The following conclusions have been deduced:

(1) In the case of carbon activated *via* physical/chemical techniques, the wet method of activation treatment for walnut shell emerges as the most optimal choice. Given its ideal specific surface area, micropore volume, and average pore size, it is well-suited for use as an adsorbent. The mixed gas activation technique comes in second, with its physical adsorption capacity being only marginally lesser than that of wet activation.

(2) The specific surface area of the ion-activated carbon fluctuates in the range of 1302.01–2214.06 $m^2\ g^{-1}$, and the micropore volume varies from 0.47 to 0.93 $cm^3\ g^{-1}$. Among them, the specific surface area of Ion-D stands at 2214.06 $m^2\ g^{-1}$, the micropore volume is 0.93 $cm^3\ g^{-1}$, and the average pore size is 1.73 nm. It showcases an excellent adsorption effect and lower production cost.

(3) Ionic activators can generate activated carbon with a high/ultra-high specific surface area. The adsorption effect of ion-activated carbons are substantially more efficient than that of physically or chemically activated carbons. Among the materials studied, Ion-D is the best, demonstrating a consistently high CIP removal rate nearing 100% at 40 °C.

(4) The shell-based ion-activated carbon exhibits an impressive regeneration cycle capacity of up to 10 cycles, with an initial regeneration efficiency of 98.64% and a final regeneration efficiency of 88.04%.

Conflicts of interest

There are no conflicts to declare.

Acknowledgements

This research was supported by National Key R&D Program of China (No. 2021YFC3001803), Key Research and Development Program of Shaanxi Province (No. 2018ZDXM-SF-033), Hubei market supervision bureau technical support project. Thanks for the support of Wang Kuancheng Foundation.

References

1 G. Xiao, R. Wu, H. Zhou, *et al.*, Preparation and Characterization of Activated Carbons Based Alkali Lignin by KOH Chemical Activation, *J. Combust. Sci. Technol.*, 2014, (8), 7–11.

2 N. E. Williams, O. A. Oba and N. P. Aydinlik, Modification, Production, and Methods of KOH-Activated Carbon, *ChemBioEng Rev.*, 2022, **9**(2), 164–189.

3 A. Sasmita and S. D. Edward, CO adsorption performance of rubber wood activated carbon, *Mater. Today*, 2022, **63**, 26–31.

4 L. B. Zhang, J. H. Peng, H. Y. Xia, *et al.*, Preparation of high specific surface area activated carbon from tobacco stem with potassium carbonate activation by microwave heating, *J. Funct. Mater.*, 2018, (01), 136–138.

5 H. Wolfgang and E. Klose, On the suitability of agricultural by-products for the manufacture of granular activated carbon, *Fuel*, 2019, **74**(12), 1786–1791.

6 J. F. González, S. Román, J. M. Encinar, *et al.*, Pyrolysis of various biomass residues and char utilization for the production of activated carbons, *J. Anal. Appl. Pyrolysis*, 2009, **85**(1–2), 134–141.

7 A. Magdziarz and M. Wilk, Thermal characteristics of the combustion process of biomass and sewage sludge, *J. Therm. Anal. Calorim.*, 2018, **114**(2), 142–145.

8 S. Román, J. F. González, C. M. González-García, *et al.*, Control of pore development during CO_2 and steam activation of olive stones, *Fuel Process. Technol.*, 2018, **89**(8), 715–720.

9 S. Deng, H. Wei, T. Chen, *et al.*, Superior CO_2 adsorption on pine nut shell-derived activated carbons and the effective micropores at different temperatures, *Chem. Eng. J.*, 2014, (08), 132–135.

10 A. Alonso, V. Ruiz, C. Blanco, *et al.*, Activated carbon produced from Sasol-Lurgi gasifier pitch and its application as electrodes in supercapacitors, *Carbon*, 2016, (3), 236–240.

11 M. F. Yu, X. B. Hu, K. C. Wang, *et al.*, KOH activation and preparation of high specific surface area of bamboo activated carbon research, *J. Zhejiang For. Sci. Technol.*, 2006, **26**(3), 17–20.

12 X. X. Zhang and S. C. Guo, The new technique to prepare high surface area activated carbon, *J. Mater. Sci. Eng.*, 2016, **14**(4), 4.

13 F. C. Wu, R. L. Tseng and R. S. Juang, Comparisons of porous and adsorption properties of carbons activated by steam and KOH, *J. Colloid Interface Sci.*, 2015, **283**(1), 49–56.

14 R. S. Juang, F. C. Wu and R. L. Tseng, Characterization and use of activated carbons prepared from bagasses for liquid-phase adsorption, *Colloids Surf., A*, 2012, **201**(1), 191–199.

15 M. Bardhan, T. M. Novera, M. Tabassum, *et al.*, Adsorption of methylene blue onto betel nut husk-based activated carbon prepared by sodium hydroxide activation process, *Water Sci. Technol.*, 2020, **82**(9), 1932–1949.

16 J. Hayashi, T. Horikawa, I. Takeda, *et al.*, Preparing activated carbon from various nutshells by chemical activation with K_2CO_3, *Carbon*, 2002, **40**(13), 2381–2386.

17 S. H. Kim, H. K. Shon and H. H. Ngo, Adsorption characteristics of antibiotics trimethoprim on powdered and granular activated carbon, *J. Ind. Eng. Chem.*, 2010, **16**(3), 344–349.

18 E. Maria, M. José, V. Eulalia, *et al.*, Comparative adsorption of ciprofloxacin on sugarcane bagasse from Ecuador and on commercial powdered activated carbon, *Sci. Total Environ.*, 2021, 750.

19 A. Pal, K. Thu, S. Mitra, *et al.*, Study on biomass derived activated carbons for adsorptive heat pump application, *Int. J. Heat Mass Transfer*, 2017, **110**, 7–19.

20 A. Pal, K. Uddin, B. B. Saha, *et al.*, A benchmark for CO_2 uptake onto newly synthesized biomass-derived activated carbons, *Appl. Energy*, 2020, **264**, 114720.

21 B. B. Saha, K. Uddin, A. Pal, *et al.*, Emerging sorption pairs for heat pump applications: an overview, *JMST Adv.*, 2019, **1**, 161–180.

22 A. Pal, H. S. Kil, S. Mitra, *et al.*, Ethanol adsorption uptake and kinetics onto waste palm trunk and mangrove based activated carbons, *Appl. Therm. Eng.*, 2017, **122**, 389–397.

23 D. C. Dumitrache, B. D. Schutter, A. Huesman, *et al.*, Modeling, analysis, and simulation of a cryogenic distillation process for 13C isotope separation, *J. Process Control*, 2022, **22**(4), 798–808.

24 M. Soleimani and T. Kaghazchi, Agricultural Waste Conversion to Activated Carbon by Chemical Activation with Phosphoric Acid, *Chem. Eng. Technol.*, 2010, **30**(5), 649–654.

25 M. Inagaki, E. Beguin and E. Frackowiak, *Carbons for Electrochemical Energy Storage and Conversion Systems*, CRC press, 2010, pp. 37–76.

26 S. Liu, *Study on adsorption of trace ethane by activated carbon with potassium hydroxide*, Dalian University of Technology, 2020.

27 E. Schroeder, K. Thomauske, C. Weber, *et al.*, Experiments on the generation of activated carbon from biomass, *J. Anal. Appl. Pyrolysis*, 2017, **79**(2), 106–111.

28 S. Román, J. F. González, C. González-García, *et al.*, Control of pore development during CO_2 and steam activation of olive stones, *Fuel Process. Technol.*, 2008, **89**(8), 715–720.

29 J. P. Feng, M. Liu, S. Y. Jia, *et al.*, Prrolidone acid ionic liquid efficiently catalyzes cellulose hydrolysis to produce glucose, *Acta Pet. Sin.*, 2012, **28**(05), 775–782.

30 H. P. Yang, R. Yan, H. P. Chen, *et al.*, Characteristics of hemicellulose, cellulose and lignin pyrolysis, *Fuel*, 2017, **86**(12), 1781–1788.
31 Q. Liu, S. Wang, Y. Zheng, *et al.*, Mechanism study of wood lignin pyrolysis by using TG-FTIR analysis, *J. Anal. Appl. Pyrolysis*, 2018, **82**(1), 170–177.
32 F. M. Mei, C. C. Fu, Q. L. Yang, *et al.*, The effect of acid functional groups of modified activated carbon on formaldehyde absorption, *Environ. Pollut. Control*, 2010, **32**(03), 18–22.
33 P. Márquez, A. Benítez, A. F. Chica, *et al.*, Evaluating the thermal regeneration process of massively generated granular activated carbons for their reuse in wastewater treatments plants, *J. Cleaner Prod.*, 2022, **366**, 132–139.
34 M. Z. M. Nasir, G. Indiran and M. A. A. Zaini, Assessment of thermal regeneration of spent commercial activated carbon for methylene blue dye removal, *Part. Sci. Technol.*, 2020, **39**(04), 503–510.